Stationary Points in Yukawa-corrected $N{+}1$ Maxwell Ring

Akshat Srivastava[1]

[1]12th grade, Narayana E-Techno School, Gurugram, India

Abstract—**We investigate the equilibrium structure and zero-velocity geometry of an $N + 1$ body ring system in which the central primary generates a Yukawa-modified gravitational potential. The modified interaction, characterized by amplitude α and screening parameter σ, generalizes the Manev-type quasi-homogeneous field by introducing a finite-range correction to the Newtonian force. Equilibria were computed numerically for $N = 3 - 100$ using a bisection-refined gradient search, and systematically compared with the Newtonian baseline. We quantify the displacement ("shift") of equilibrium positions and map bifurcation regions in the (α, σ, β) parameter space. The results show that while the Newtonian five-family structure persists for moderate parameters, new equilibrium pairs emerge or disappear within narrow windows of α and σ. Zero-velocity curves confirm these saddle-node transitions through the appearance of new potential wells and connectivity changes. All equilibria remain linearly unstable. The analysis provides a quantitative baseline for understanding finite-range and screened-gravity effects in ring-type dynamical systems.**

Keywords: Yukawa potential, equilibria, zero-velocity curves, bifurcations, $N + 1$ ring

I Introduction

The dynamics of N+1 body configurations arranged in polygonal or ring-type geometries have been studied extensively since Maxwell's work on the stability of Saturn's rings [1]. In the classical Newtonian case, such systems exhibit a rich equilibrium structure comprising up to five distinct families of stationary points, whose properties depend on the number of peripheral bodies N and the mass ratio between the ring and central primary β. Analyses by Kalvouridis, Elipe, and others have described these families and their zero-velocity geometry in detail [2], [3].

However, several physical scenarios motivate deviations from the strict $1/r$ potential. Finite-range gravitational interactions arise in modified-gravity and screened-gravity models (Yukawa, f(R), scalar-tensor) [4], in radiating or oblate primaries, and in plasma or granular analogs where effective inter-particle forces decay exponentially. A significant body of work has extended the ring problem to such quasi-homogeneous potentials, including the Manev-type field [5], [6]. The corresponding potential can be represented as

$$V = -\frac{Gm}{r}(1 + \alpha e^{-\sigma r})$$

where α measures the strength of the correction and σ^{-1} measures its range. The Yukawa correction has been shown to significantly alter the dynamics of three-body systems [4] and ring configurations [6].

The purpose of this study is to examine how such Yukawa-type corrections alter the equilibrium configurations, zero-velocity surfaces [7], and stability properties of the ring problem. Building on the normalized potential formulation introduced by Kalvouridis [2], we systematically compute the equilibria and bifurcation patterns in the modified potential, analyze the parameter dependence of their shifts, and identify parameter domains where new equilibria appear or vanish [4]. The results provide both a generalization of classical ring dynamics and a computational reference for studying finite-range interactions in planetary rings and related systems.

II Model

Consider a ring arrangement of the primaries, one at the center and the others at the vertices of the regular N-sided polygon. We adopt non-dimensional units where the ring radius and masses of the peripheral primaries are unity. The mass of the central primary is characterized by the parameter β.

Let (r, θ) be polar coordinates in the rotating frame. The modified pairwise interaction uses a Yukawa-corrected kernel:

$$h(r) = 1 + \alpha\, e^{-\sigma r}, \qquad f(r) = \frac{h(r)}{r}.$$

Here α is the Yukawa amplitude and $\sigma > 0$ the screening length inverse. Thus the gravitational potential due to a mass m at a distance r from it will be

$$V(r) = -Gm\, f(r)$$

Similarly to the newtonian case, as discussed by Kalvouridis in [2], the reduced potential per unit mass is

$$U(r, \theta) \;=\; \frac{1}{\Delta(\alpha)}\Big(\beta f(r) + \sum_{j=0}^{N-1} f(r_j)\Big) + \tfrac{1}{2} r^2, \quad (1)$$

where $r_j = \sqrt{r^2 + 1 - 2r\cos(\theta - \theta_j)}$, $\theta_j = 2\pi j/N$, and

$$\Delta = -b\,\partial_r f(1) - \sum_{j=1}^{N-1} \partial_r f\big(2\sin(\tfrac{\pi j}{N})\big)\,\sin(\tfrac{\pi j}{N})$$

is the normalizing factor.

The Jacobi constant is defined as $C = 2U - v^2$ and zero-velocity curves correspond to constant C level sets with $v = 0$, providing valuable information about permissible motion regions [7].

III Stationary solutions

The equilibria points are those which are at rest in the rotating frame. These satisfy $\nabla U(r, \theta) = 0$.

Due to the symmetrical nature of the problem, all the equilibria will lie on the radial lines corresponding to $\theta = n\pi/N$ $(n \in \mathbb{Z})$, the lines joining the central and peripheral primaries or the angle bisectors of these. The equilibria can be identified by locating zeroes of the radial gradient component $\partial_r U(r, \theta)$ for these values of θ.

Based on the location of the points, they can be divided into 5 zones, analogous to the collinear and triangular Lagrange points in the three-body problem [8]:

- Zone A_1 is the closest to the origin, containing the stationary points which lie on the lines connecting the central and a peripheral primary and are located between them. These points are known as inner collinear points.
- Zone A_2 is the second closest, containing the stationary points which lie on the bisector between two successive peripheral primaries and are between the central and peripheral primaries. These points are known as inner between-masses points.
- Zone B includes the stationary points which lie on the same bisector but are between two successive peripheral primaries. These points are known as peripheral between-masses points.
- Zone D_2 contains the stationary points which lie on the bisector between two consecutive peripheral primaries, but beyond them. These points are known as outer island points.
- Zone D_1 contains the stationary points that lie on the lines connecting the central and a peripheral primary, located beyond them. These points are known as outer collinear points.

There can be a minimum of three and maximum of all five zones present, each containing N equilibrium points.

IV Numerical methods

IV-A Equilibrium detection

The equilibria can be identified by locating zeroes of the radial gradient component $\partial_r U(r, \theta)$ for θ values of $\theta = $

$n\pi/N$ $(n \in \mathbb{Z})$.

The computation proceeds as follows:

1) Grid initialization: Sample the radial coordinate on a uniform grid $r \in [\varepsilon, r_{\max}]$ with $n_r = 100$ points, where $\varepsilon = 10^{-12}$ avoids the central singularity and $r_{\max} = 2.5$.
2) Gradient computation: Compute $\partial_r U(r, \theta)$ at all grid points simultaneously.
3) Detection of sign-changes: Identify intervals $[r_i, r_{i+1}]$ where $\mathrm{sgn}(\partial_r U(r_i, \theta)) \neq \mathrm{sgn}(\partial_r U(r_{i+1}, \theta))$, indicating a root by the intermediate value theorem.
4) Root refinement: For each detected interval, apply the iterative bisection method (maximum 50 steps) to refine the location of the root until $|\partial_r U(r, \theta)| < \tau = 10^{-5}$.

This approach avoids expensive nonlinear solvers. This was used to find roots both in the modified case and Newtonian case. Corresponding equilibria were compared to find shifts in their locations.

IV-B Zero velocity curves

The Jacobi constant $C(r, \theta; v) = 2U(r, \theta) - v^2$ defines forbidden regions for a given energy level. To visualize these:

1) Grid construction: Generate a Cartesian grid $(x, y) \in [-0.1, 2.5]^2$ with 200×200 points and convert to polar coordinates (r, θ) via $r = \sqrt{x^2 + y^2}$, $\theta = \arctan 2(y, x)$.
2) Contour plotting: Plot level curves of $C(x, y; 0)$ for both Newtonian ($\alpha = 0$, black dashed) and modified ($\alpha > 0$, green solid) cases on the same axes, with equilibria overlaid as colored markers.

IV-C Performance optimization

Key computational accelerations include:

1) JIT compilation: All core functions (U, ∇U, Hessian) were decorated with `@njit` for native machine code generation via Numba's LLVM backend.
2) Vectorization: Used numpy vectorization to calculate (U, ∇U, Hessian) for a whole array at once.

For a typical sweep over $(\alpha, \sigma, \beta) \in [0, 20] \times [0, 5] \times [\beta_{\min}, \beta_{\max}]$ with $50 \times 50 \times 80 = 200{,}000$ grid points, parallel execution on an 16-core processor completes in ~ 5 minutes per N-value.

V Results

V-A Newtonian baseline

For $\alpha = 0$ the equilibrium structure is that of the classical (Newtonian) $N + 1$ body problem. Depending on N and the central mass parameter β the unperturbed problem reproduces the stationary points discussed in [2], [3]:

regimes with $3N$, $4N$ or $5N$ distinct equilibria occur as β is varied.

V-B Shift vs parameters

We quantify the shift of equilibria by the Euclidean displacement between Newtonian and modified equilibria, $\Delta r = \|\mathbf{x}_{\text{mod}} - \mathbf{x}_{\text{newt}}\|$, computed for matched symmetry-angle solutions when available. As shown in Figures 1 and 5, key empirical trends include:

- Increasing α: Δr increases monotonically at small-to-moderate α and tends to saturate at large α where the Yukawa correction dominates the local potential near the ring masses, consistent with findings in modified potential studies [4], [6].
- Varying β: the response is non-monotonic; for small β the central mass is weak and ring-induced shifts dominate, while for large β the central potential constrains displacements and competing effects produce local extrema in $\Delta r(\beta)$.
- Varying σ: larger σ (stronger screening) localizes the modification and typically reduces long-range coupling, yielding smaller Δr for fixed α, as expected from the finite-range nature of Yukawa corrections [4].

All shift statistics reported below are averaged over matched equilibrium pairs found by `calc_shifts_vectorized`; error bars indicate the sample standard deviation across matched points.

V-C Bifurcation maps and creation of equilibria

We construct bifurcation maps by comparing the number of equilibria in the modified potential ($\alpha > 0$) to the Newtonian baseline ($\alpha = 0$) on a discrete (α, σ, β) grid. The signed difference $\Delta n \equiv n_{\text{mod}} - n_{\text{newt}}$ is used as the map value; contiguous regions with $\Delta n = \pm 2$ identify saddle-node windows where a pair of equilibria is created ($\Delta n = +2$) or destroyed ($\Delta n = -2$).

Figure 2 shows a representative α–σ sweep for $N = 6$, $\beta = 2.0$. This case, where the Newtonian potential already supports $3N$ equilibria [2], [3], is dominated by yellow/red regions ($\Delta n = 2$), indicating that the Yukawa correction primarily creates new equilibrium pairs. These creation windows form intricate, narrow bands in the parameter space.

V-D Disappearance of equilibria for small N

For small numbers of peripheral bodies, the Yukawa correction can have the opposite and more dramatic effect of *reducing* the total number of equilibria. This is particularly pronounced for $N = 3$ and $N = 4$, where the Newtonian potential can support the full $5N$ equilibria for sufficiently small β [3].

Figure 6 displays α-σ bifurcation maps for $N = 3$ and $N = 4$ at fixed β values chosen to be within the Newtonian $5N$ regime. The prominent red regions ($\Delta n = -2$) indicate where the modified potential sustains fewer equilibrium points than the Newtonian baseline—entire families (zones A_2 and B) vanish. For $N = 3$, the disappearance occurs along a narrow, convoluted filament in (α, σ) space, while for $N = 4$, the region of destruction is broader. This phenomenon, where finite-range corrections annihilate existing Lagrange-point analogs, has no counterpart in the classical problem and underscores the non-perturbative impact of the Yukawa term on the potential topology for small N.

V-E Three-dimensional bifurcation structure

In addition to 2D slices we constructed 3D bifurcation volumes as shown in Figure 4. This visualization encapsulates the complex interplay where, depending on N and β, the Yukawa parameters can create new equilibria, destroy existing ones, or both in different regions of the (α, σ, β) space.

V-F Zero Velocity Curves

Zero-velocity curves (ZVCs) illustrate how allowed regions change topologically across a bifurcation event [7]. For each illustrative panel we plot paired contours of the Jacobi constant $C = 2U - v^2$: Newtonian contours (dashed black) versus modified contours (solid green). Equilibria are marked (blue for Newtonian, red for modified) and annotated with their (r, θ) coordinates.

Figure 3 presents a typical case. The panels demonstrate how the Yukawa modification can create or destroy small pockets or channels in the ZVC, corresponding to the emergence or disappearance of equilibrium points in different zones, similar to topological changes observed in ring problems with modified potentials [5], [7].
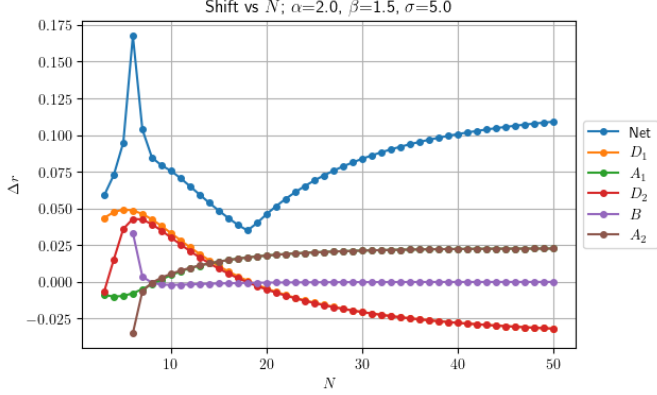
VI   Figures and Analysis

Fig. 1: Shift in equilibrium radial distance (Δr) as a function of the number of peripheral bodies N. Parameters are fixed at $\alpha = 2.0$, $\sigma = 5.0$, $\beta = 1.5$. The shift is calculated for equilibria in zone A_1 (inner collinear points). The non-monotonic trend highlights the complex interplay between the Yukawa correction and the ring's self-gravity, which changes discretely with N.
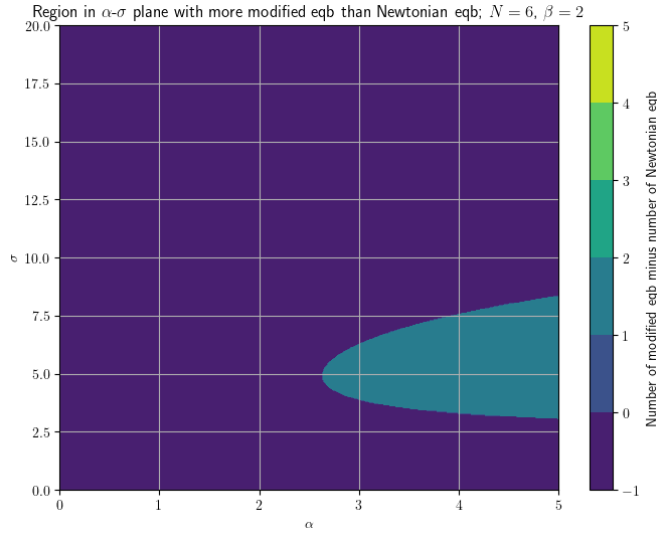

Fig. 3: Example Zero-Velocity Curve (ZVC) for $N = 6$, $\beta = 2.0$, $\alpha = 2.0$, $\sigma = 5.0$. The Jacobi constant level is set to $C = 2U(r_{\text{eq}}, 0)$. The solid green contour (Yukawa-modified) is compared to the dashed black contour (Newtonian). The modified potential alters the topology of the forbidden region (exterior of the contour) and creates a new, isolated potential well (small green lobe near $x \approx 1.2, y \approx 0$), which corresponds to a newly bifurcated equilibrium point not present in the Newtonian case. Equilibrium points are marked by stars (Newtonian: blue, Yukawa: red).

Fig. 2: Bifurcation map in the α-σ parameter plane for $N = 6$, $\beta = 2.0$. The color indicates the change in the number of equilibria ($\Delta n = n_{\text{mod}} - n_{\text{newt}}$) relative to the Newtonian baseline. Yellow/red regions ($\Delta n = 2$) indicate where new equilibrium pairs appear via saddle-node bifurcations. Blue regions ($\Delta n = -2$) indicate where pairs vanish. The intricate structure reveals critical parameter windows for topological changes in the equilibrium set.
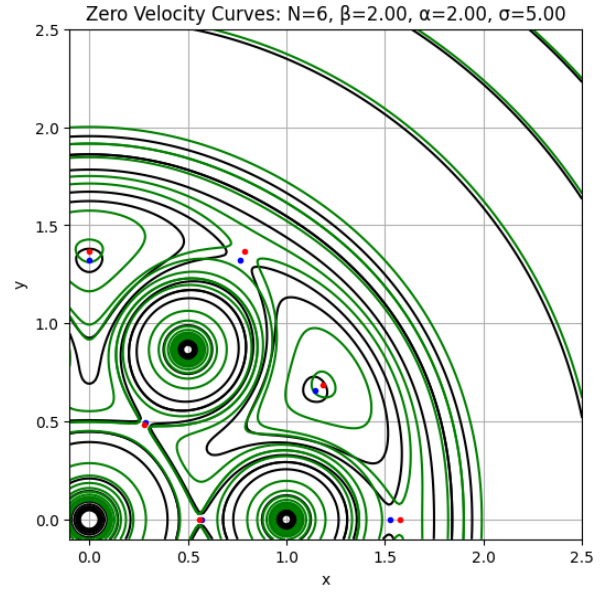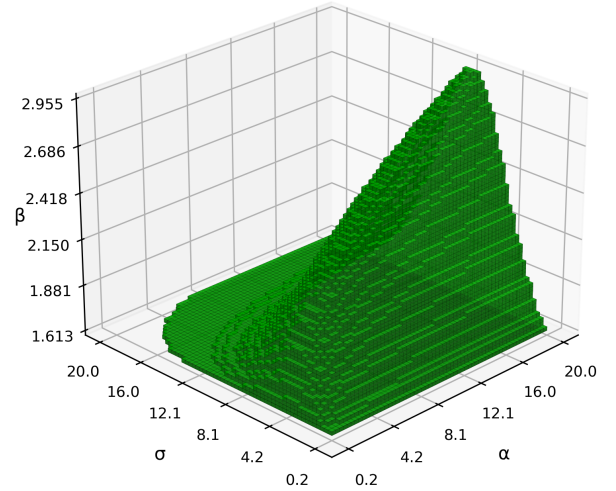

Fig. 4: Three-dimensional bifurcation volume for $N = 6$, showing (α, β, σ) regions where $\Delta n = 2$. The irregular surface topology highlights complex interdependence between Yukawa parameters and mass ratio. Slices at constant β yield two-dimensional maps as in Fig. 2.
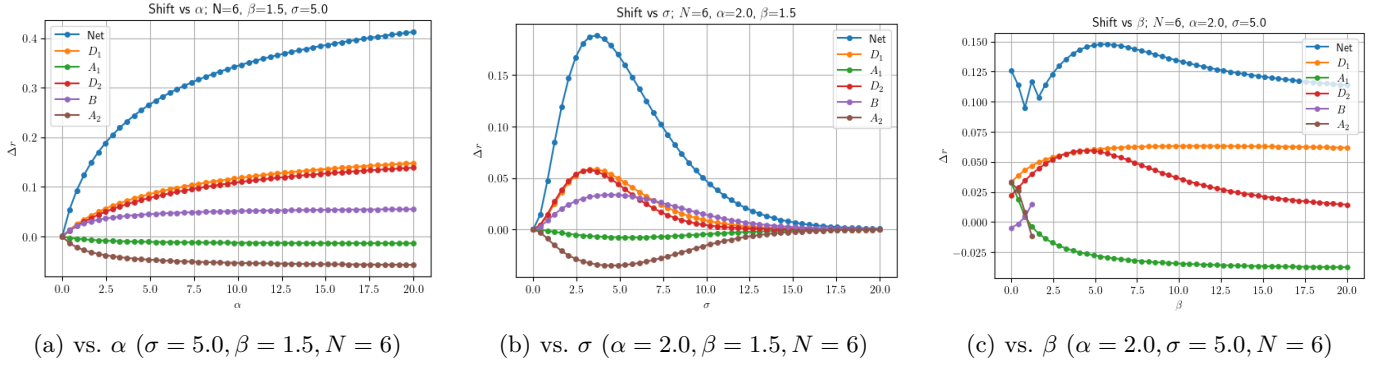
(a) vs. α ($\sigma = 5.0, \beta = 1.5, N = 6$)   (b) vs. σ ($\alpha = 2.0, \beta = 1.5, N = 6$)   (c) vs. β ($\alpha = 2.0, \sigma = 5.0, N = 6$)

Fig. 5: Radial shift Δr of zone A_1 equilibria as a function of individual Yukawa and system parameters for $N = 10$. (a) Shift increases and saturates with Yukawa strength α. (b) Shift decays exponentially with screening parameter σ, reflecting the finite-range nature of the correction. (c) Non-monotonic dependence on central mass β, showing competition between central and ring potentials.
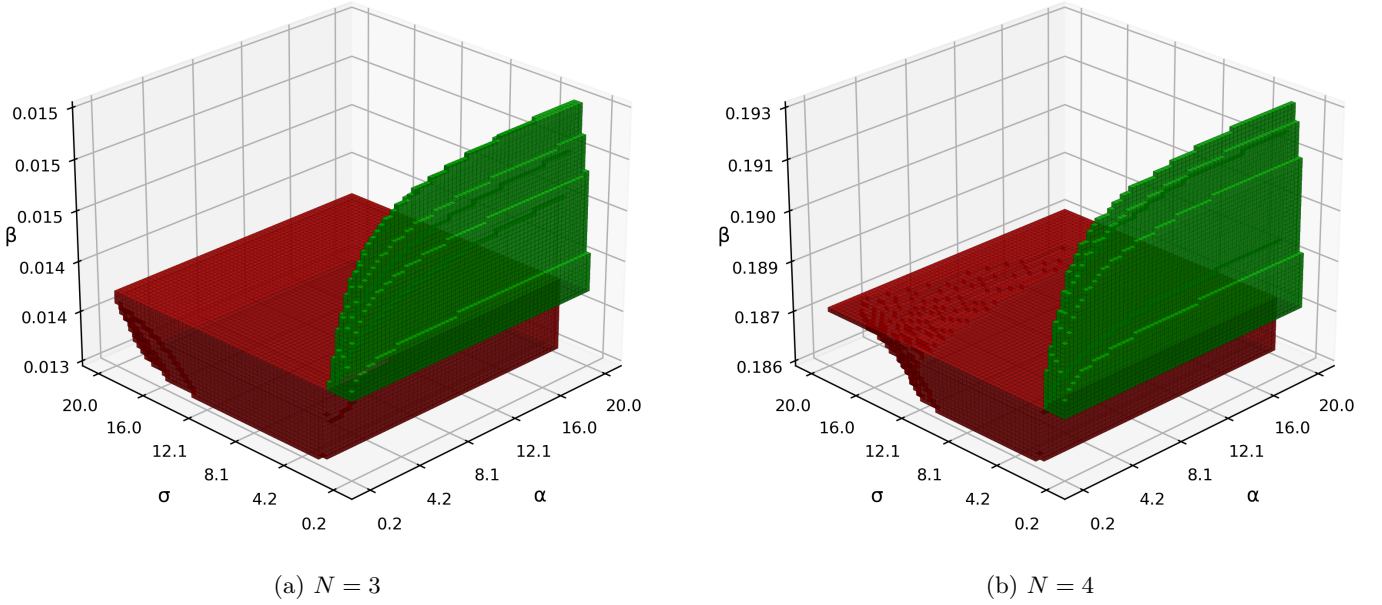

(a) $N = 3$ (b) $N = 4$

Fig. 6: Bifurcation maps in the α-σ plane showing regions where the Yukawa-modified potential has *fewer* equilibria than the Newtonian case ($\Delta n = -2$, red). The fixed β values are chosen so that the Newtonian baseline ($\alpha = 0$) is in the $5N$ regime [3]. For $N = 3$ (a), the intricate red filament shows where an entire equilibrium family vanishes. For $N = 4$ (b), broader red regions indicate parameter spaces where two families disappear. This contrasts with the creation-dominated maps for larger N (Fig. 2).

VII   Conclusion

Finite-range Yukawa corrections to the point-mass potential produce systematic, quantifiable shifts of equilibrium positions in the $N + 1$ ring system. More significantly, they generate narrow but robust parameter windows where saddle-node bifurcations add or remove equilibrium pairs [4]. These bifurcation windows, mapped in the $(\alpha, \sigma, \beta, N)$ space, vary predictably with system parameters and are corroborated by topological changes in the zero-velocity curves [7]. First-order perturbation theory provides a reliable quantitative prediction for small α ($\alpha \lesssim 0.1$) but fails near bifurcation folds. While all discovered equilibria in the Yukawa-modified field remain linearly unstable—similar to the collinear Lagrange points in the classical three-body problem [8]—their altered locations and the very existence of new equilibrium families have implications for particle trapping and the long-term evolution of ring structures under screened-gravity potentials. Limitations of the present study include planar geometry, point-mass

primaries and omission of dissipative forces. Future work will pursue higher-order asymptotics, rigorous continuation using numerical continuation techniques, and extension to fully three-dimensional setups as studied in [7], [6].

Acknowledgments

References

[1] J. C. Maxwell, *On the Stability of the Motions of Saturn's Rings*. Cambridge: Macmillan and Company, 1859.

[2] T. J. Kalvouridis, "A planar case of the $n+1$ body problem: The 'ring' problem," *Astrophysics and Space Science*, vol. 260, no. 3, pp. 309–325, 1999.

[3] Z. Boureghda, M. C. Martinez-Belda, and J. F. Navarro, "Analysis of the geometry of the zero-velocity curves in the n-body ring problem depending on the mass ratio parameter," *The European Physical Journal Plus*, vol. 139, no. 1, p. 69, 2024.

[4] F. Kokubun, "Restricted problem of three bodies with newtonian + yukawa potential," *International Journal of Modern Physics D*, vol. 13, no. 5, pp. 783–806, 2004.

[5] D. G. Fakis and T. J. Kalvouridis, "On a property of the zero-velocity curves in the regular polygon problem of $n+1$ bodies with a quasi-homogeneous potential," *Celestial Mechanics and Dynamical Astronomy*, vol. 116, no. 3, pp. 229–253, 2013.

[6] X. Xu, "On the vertical libration of maxwell's ring configuration with a manev potential," *Journal of Nonlinear Mathematical Physics*, vol. 31, p. 81, 2024.

[7] T. J. Kalvouridis, "Zero-velocity surfaces in the three-dimensional ring problem of $n+1$ bodies," *Celestial Mechanics and Dynamical Astronomy*, vol. 80, no. 2, pp. 133–144, 2001.

[8] V. Szebehely, *Theory of Orbits*. New York: Academic Press, 1967.